Dalton Transactions

This article can be cited before page numbers have been issued, to do this please use: E. E. Hardy, M. A. Eddy, B. A. Maynard and A. E. V. Gorden, *Dalton Trans.*, 2016, DOI: 10.1039/C6DT02389D.

View Article Online
DOI: 10.1039/C6DT02389D

Journal Name

ARTICLE

Solid State π–π Stacking and Higher Order Dimensional Crystal Packing, Reactivity, and Electrochemical Behaviour of Salphenazine Actinide and Transition Metal Complexes

Received 00th January 20xx,
Accepted 00th January 20xx

DOI: 10.1039/x0xx00000x

www.rsc.org/

E. E. Hardy,[a] M. A. Eddy,[a] B. A. Maynard[a] and A. E. V. Gorden[a]

Condensation of a 2,3-diaminophenazine or 2,3-diamino-2-quinoxalinol with two equivalents of 3,5-ditertbutylsalicylaldehyde affords new Schiff base ligands. Here, we describe and compare the synthesis, UV-Vis, electrochemical, solution, and solid state behaviour of the free base, salphenazine ligand [L^{I}], and M[L^{I}] complexes, where M = UO_2(VI), Cu(II), VO(IV), Zn(II), Co(II), and Ni(II). The change in π-overlap and π-stacking between molecules and long-range ordering of the solid-state structure is vastly different depending on the size and electronic character of the metal. A sterically constrained μ-oxo Fe(III) dimer complex is also reported.

Introduction

Nuclear power and nuclear medicine are two potential applications of actinide elements.[1] The isolation of actinides for nuclear fuels and accidental spills have introduced actinides into the environment and raised concerns about health effects.[2] Rapid in-the-field identification and isolation could greatly improve the ease of remediation.[3] Schiff base-type ligands with an O-N-N-O coordination core have been investigated in numerous applications[4] including: catalysis,[5] antimicrobial assays,[6] in organic light emitting diodes,[7] and in fluorescent or colorimetric sensors.[8a-c] Salen metal complexes are of interest in these and other applications due to the relative ease of introducing functionality while maintaining a simple synthetic approach.[8b] Preparation of metal complexes using metal templation reduces the potential of additional side products while maintaining high yields.[9]

Actinides are present at low concentrations in soils and wastewater streams.[10] In comparison, transition metals are present at much higher concentrations, and the transition metals can compete with f-elements for coordination sites.[11] This can complicate the rational design of ligands for actinide selective coordination; in particular, the highly electropositive copper has been found to yield a false positive result in ligands designed to selectively isolate or detect uranyl (UO_2^{2+}).[12] The O-N-N-O binding coordination pocket of the Salqu ligand [L^{II}] with an extended conjugated heterocycle (2-quinoxolinol) incorporated into the backbone accommodates the preferential equatorial pentacoordinate binding geometry of the uranyl dication. This, coupled with the imine nitrogen soft donor, improves binding of actinides as compared to lanthanides, which can tend to form polymeric aggregates.[13,14]

The salphenazine [L^{1}] ligand features the further extended phenazine backbone and a distinct hypsochromic shift with the coordination of uranyl dication (UO_2^{2+}). This is very distinct from the bathochromic shift seen in the complexes with transition metals.[15,16] Here, we report the detailed characterization of salphenazine [L^{1}] and comparable salqu [L^{II}] metal complexes in solids by X-ray diffraction, in solution spectroscopy, and electrochemistry.

Materials and Methods

General Synthetic Details

Caution! The uranium metal salts - $UO_2(NO_3)_2$•$6H_2O$ - used in this study contained depleted uranium, standard precautions for handling radioactive materials or heavy metals, such as uranyl nitrate and lead sulfate, were followed.

The reagents 1,5-difluoro-2,4-dinitrobenzene (97%, Matrix Scientific), leucine methyl ester hydrochloride (TCI), diisopropylethylamine (Aldrich), ammonium hydroxide (BDH), ammonium formate (97%, Aldrich), palladium 5% on carbon, dry, type 87L (Alpha Aesar), 3,5-di-tert-butylsalicyaldehyde (98%, TCI), 2,3-diaminophenazine (98%, Aldrich), copper (II) acetate hydrate (>98%, MC/B), copper (II) acetylacetonate (98% STREM), vanadium (IV) bis(acetylacetonato)oxide (98%, STREM), cobalt (II) acetate tetrahydrate (Mallinckrodt), nickel (II) acetate tetrahydrate (Aldrich), zinc acetate dehydrate (Aldrich) and tetra-n-butylammonium perchlorate (Alfa Aesar, electrochemical grade) were used as received without further purification. $UO_2(NO_3)_2$•$6H_2O$ (98%, J. T. Baker) was recrystallized from an aqueous nitric acid solution, stored

---

[a] Department of Chemistry and Biochemistry, Auburn University, 179 Chemistry Building, Auburn, Alabama 36849, USA. anne.gorden@auburn.edu

Electronic Supplementary Information (ESI) available: [details of any supplementary information available should be included here]. See DOI: 10.1039/x0xx00000x

View Article Online
DOI: 10.1039/C6DT02389D

under hexanes and washed and dried before use. THF (BDH), chloroform (BDH), ethyl acetate (BDH), hexanes (BDH), acetone (BDH) and pyridine (anhydrous, Aldrich) were used as received with no further purification.

UO$_2$[L^I] and **Cu[L^I]** salphenazine metal complexes were prepared using metal templation methods.[16] Synthesis of 6,7-diamino-2-quinoxalinol and 3,5-ditertbutylsal-2-quinoxalinol (salqu) **[H$_2$L^{II}]**, **UO$_2$[L^{II}]**, and **Cu[L^{II}]** were prepared using metal templation.[13a,17] Purity was confirmed by HRMS and NMR spectroscopy.

VO[L^I] 2,3-diaminophenazine (231 mg, 1.10 mmol) was dissolved in 35 mL of pyridine and added slowly to a round bottom flask containing 3,5-ditertbutylsalicylaldehyde (507 mg, 2.17 mmol), vanadium (IV) bis(acetylacetonato)oxide (281 mg, 1.06 mmol), 20 mL of pyridine, and a stir bar. The reaction vessel was heated to 80 °C for 24 hours. The solvent was removed using a rotary evaporator, and the remaining solid dried in a vacuum oven at 60 °C overnight. This crude solid was purified using column chromatography (2:1 hexanes:ethyl acetate). Yield: 27.4 %; red crystals were grown from slow diffusion of methanol into a saturated solution in THF. CCDC: 1452867. HRMS (EI) m/z (M+H) calcd 708.3166, found 708.3269.

Zn[L^I] 2,3-diaminophenazine (197 mg, 0.940 mmol) was dissolved in 35 mL of pyridine and subsequently added slowly to a round bottom flask containing 3,5-ditertbutylsalicylaldehyde (505 mg, 2.18 mmol), zinc acetate dihydrate (237 mg, 1.04 mmol), 20 mL of pyridine, and a stir bar. The reaction vessel was heated to 80 °C for 24 hours. The solvent was removed using a rotary evaporator, and the remaining solid was dried in a vacuum oven at 60 °C overnight. This crude solid was purified using column chromatography (2:1 hexanes:ethyl acetate). Yield: 24.2 %; red crystals were grown from slow diffusion of methanol into a saturated solution in THF. CCDC: 1452244. Metal complex formation was confirmed via UV spectroscopy, λ_{max} = 387 nm (ε = 1.79 x 10^4 cm^{-1} M^{-1}) and 521 nm (ε = 1.51 x 10^4 cm^{-1} M^{-1}). IR spectroscopy, 3417.92(m), 2955.96(m), 1612.52(s), 1595.16(s), 1432.17(m), 1383.9(m), 1164.06(m), 1128.38(m), 1026.15(w), 983.71(w), 908.49(w), 870.88(w), 755.14(m), 677.99(w) cm^{-1}. HRMS (EI) m/z: (M+H) calcd 705.3069, found 643.3734. The HRMS matrix was found to be acidic and stripped the zinc out of the complex. The observed ion at 643.3734 m/z indicates the presence of the protonated free base.

Fe[L^I]-O-Fe[L^I] 2,3-diaminophenazine (211 mg, 1.01 mmol) was dissolved in 35 mL of pyridine and subsequently added slowly to a round bottom flask containing 3,5-ditertbutylsalicylaldehyde (540. mg, 2.31 mmol), iron (III) trichloride hexahydrate (277 mg, 1.03 mmol), 20 mL of pyridine, and a stir bar. The reaction vessel was heated to 80 °C for 24 hours. The solvent was removed using a rotary evaporator. The remaining solid was dried in a vacuum at 60 °C oven overnight. The resulting crude solid was purified using column chromatography (4:3 hexanes:acetone). Yield: 21.2 %; red crystals were grown from slow evaporation of mobile phase. CCDC: 1018600. The dimer dissociates in acidic solution to [FeL^I]$^+$. HRMS (EI) m/z: (M$^+$) calcd 696.3127, found 696.3117.

Co[L^I] 2,3-diaminophenazine (201 mg, 0.958 mmol) dissolved in 35 mL of pyridine was added slowly to a round bottom flask containing 3,5-ditertbutylsalicylaldehyde (541 mg, 2.31 mmol), cobalt (II) acetate hydrate (220. mg, 0.885 mmol), 20 mL of pyridine, and a stir bar. The reaction vessel was heated to 80 °C for 24 hours. The solvent was removed using a rotary evaporator, and the remaining solid was dried in a vacuum oven at 60 °C overnight. The resulting crude solid was purified using column chromatography (4:3 hexanes:acetone). Yield: 20.1 % HRMS (EI) m/z: (M+H) calcd 699.3109, found 699.3079.

Ni[L^I] 2,3-diaminophenazine (190. mg, 0.904 mmol) was dissolved in 35 mL of pyridine and added slowly to a round bottom flask containing 3,5-ditertbutylsalicylaldehyde (485 mg, 2.07 mmol), nickel (II) acetate hydrate (193 mg, 0.778 mmol), 20 mL of pyridine, and a stir bar. The reaction vessel was heated to 80 °C for 24 hours. The solvent was removed using a rotary evaporator, and the remaining solid was dried in a vacuum oven at 60 °C overnight. The crude solid was purified using column chromatography (2:1 hexanes:ethyl acetate). The mobile phase was evaporated under reduced pressure to yield a dark red solid. Yield: 36.9 %. HRMS (EI) m/z: (M+H) calcd 699.3209, found 699.3221.

[H$_2$L^I] (salphenazine) UO$_2$[L^I] (100 mg) was dissolved in 20 mL of THF and added to 60 mL of chloroform. Nitric acid (80 mL, 1M) was added to the red organic phase in a separatory funnel. The organic layer was washed a second time with deionized water (80 mL). The yellow organic layer was evaporated under reduced pressure and the ligand was separated from the monosubstitued side product via column chromatography (2:1 hexanes:ethyl acetate). Yield: 40%; orange crystals were grown from slow evaporation of the mobile phase. Products were confirmed via mass spec analysis HRMS (EI) m/z: (M+H) calcd 643.3934, found 643.3942. CCDC: 1452415.

Crystallographic Details

Datasets were collected on a Bruker SMART APEX CCD X-ray diffractometer unit using Mo Kα radiation, from crystals mounted in Paratone-N oil on glass fibers. SMART (v 5.624) was used for preliminary determination of cell constants and data collection control. [H$_2$L^I], Zn[L^I] and Fe[L^I]-O-Fe[L^I] datasets were collected at 180K, VO[L^I] dataset was collected at 296K. Determination of integrated intensities and global cell refinement were performed with the Bruker SAINT software package using a narrow-frame integration algorithm. The program suite SHELXL (v 5.1) was used for space group determination, structure solution, and refinement.[18] Refinement was performed against F^2 by weighted full-matrix least squares, and empirical absorption correction (SADABS) was applied.[19] The olex2.refinement package using Gauss-Newton minimization was used for further refinement and to generate a solvent mask to account for the 3 methanol molecules in the unit cell of VO[**L^I**]. and for 2 interstitial THF

View Article Online
DOI: 10.1039/C6DT02389D

molecules in the unit cell of $Zn[L^I]$.[20] SQUEEZE was used to remove 1.5 THF molecules from the unit cell of $Fe[L^I]$-O-$Fe[L^I]$. Projections were generated using the Olex2.1-1 graphics program.[20]

Spectroscopic Details

UV-Vis experiments were performed on a Varian Cary 50 WinUV Spectrophotometer. Solutions for each titration were made individually and stirred for 5 minutes before data collection.

Electrochemical Details

Cyclic voltammetry experiments were performed using an AFCBP1 bipotentiostat driven by a PC with the Aftermath software package. All experiments were completed with a Pt disk working electrode, a Pt wire counter electrode, and an Ag/AgCl reference electrode (BASi MF-2052). Solutions for cyclic voltammetry experiments were 1.0 mM in the salqu metal complex or ligand ($M[L^{II}]$ and $[H_2L^{II}]$), or 0.5 mM in the salphenazine metal complex or ligand ($M[L^I]$ and $[H_2L^I]$). All solutions were made in dichloromethane and contained 0.1 M tetra-n-butylammonium perchlorate (TBAP). Platinum electrodes were cleaned with piranha acid (H_2SO_4/H_2O_2), polished in between experiments, and all electrodes were stored according to factory suggestion. All experiments were performed at room temperature.

Results and Discussion

Solid State

The condensation of 2,3-diaminophenazine with two equivalents of 3,5-ditertbutylsalicylaldehyde was employed to prepare are series of 1:1 metal:ligand complexes $M[L^I]$ in good yields (20 - 36 %). The use of metal templation to prepare the metal complexes limits the formation of an imidazole 2-(1H-imidazo[4,5-b]phenazin-2-yl)phenol side product. This templation synthetic scheme (**Scheme 1**) was used to prepare the salphenzaine $M[L^I]$ complexes where M = UO_2(VI), Cu(II), VO(IV), Zn(II), Fe(III), Co(II), and Ni(II). The preparation of the free-base form of $[H_2L^I]$ in quantity both large enough and pure enough for further studies required stripping the coordinating metal from the complex using a nitric acid wash. The free-base was dissolved in chloroform, and washed with 1 M HNO_3. The organic phase was then washed three times with water and then a brine solution, followed by evaporation under reduced pressure. Finally, the free-base was separated from the monosubstitued 2-(1H-imidazo[4,5-b]phenazin-2-yl)phenol product via column chromatography.

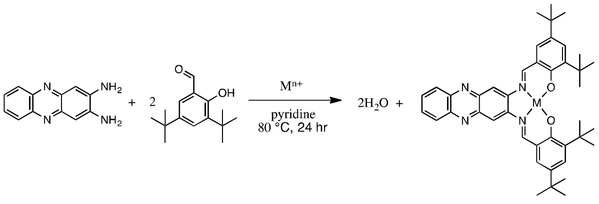

Scheme 1. Metal templated synthesis of salphenazine complexes $M[L^I]$.

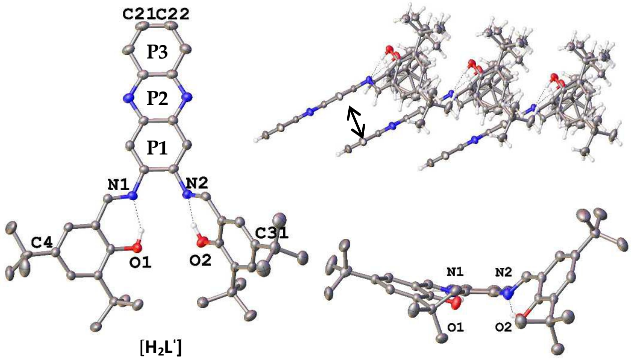

Figure 1. Salphenazine $[H_2L^I]$ crystal structure. Carbon atoms shown in grey, nitrogen shown in blue, oxygen shown in red, hydrogen atoms and interstitial ethyl acetate removed for clarity. Solid-state π– π interactions are highlighted in this projection

The structures of the free-base form of ligand $[H_2L^I]$ has been characterized by single crystal X-ray diffraction. Crystallographic details of ligands and metal series are listed in **Table 1** and important bond distances and angles are listed in **Table 2**. The ligand $[H_2L^I]$ crystallizes in the monoclinic space group $P2_1/n$. Structural representations of $[H_2L^I]$ is shown in **Figure 1**. The π–π distance between the P1-P3 rings, also depicted in Figure 1, is 3.471 Å. Of note is the non-planarity of the tetradentate binding pocket. This is counterintuitive from the highly conjugated system; however, the bond distances are such that repulsion of the two oxygen atoms distorts the planarity of the extended π-conjugated network. One phenol oxygen atom is almost in plane with the phenazine backbone while the second distorts from planarity significantly, distances above the plane are O1-plane = 1.054(2) Å and O2-plane = 0.316(2) Å. The binding of a metal to the binding pocket causes a significant change in π-overlap, which can be observed by the change in the electronic spectra of both ligands. In particular, the yellow solution of $[H_2L^I]$ turns red in the presence of common first row transition metals while it turns an orange color in the presence of uranyl, the coordination of which more greatly disturbs the planarity of conjugation. When a metal is bound, the electronic repulsion of the phenol oxygen is eliminated. The smaller ionic radii of transition metals allows for more pi orbital overlap as compared to uranyl, causing a bathochromic shift of the charge transfer band. Complex $VO[L^I]$, shown in **Figure 2**, crystallizes in the triclinic space group $P\bar{1}$. This complex has a distorted square pyramidal geometry with the axial position being an oxo group on the vanadyl cation (VO^{2+}). The geometry of the metal in the binding pocket is indicated by the bond angles of O1-V-N1, N1-V-N2, N2-V-O2, O2-V-O1 of 86.94(8), 78.27(8), 87.31(8), and 86.90(7)° respectively, comparable to other vanadyl salen and salophen complexes (N1-V1-N2 77.3-78.7° and O1-V-N1, N2-V-O2, O2-V-O1 (86.3-88.8°).[21] The $VO[L^I]$ complex is skewed from square pyramidal geometry as compared to the $Zn[L^I](CH_3OH)$ and $Fe[L^I]$-O-$Fe[L^I]$ complexes, both of which are also square pyramidal geometries. The vanadium atom V-N1

View Article Online
DOI: 10.1039/C6DT02389D

and V-N2 bond distances are 2.050(2), 2.054(2) Å, respectively. These bond lengths are comparable to others in the literature (2.05-2.07 Å) for salen type complexes, but the lack of symmetry in the angles is unusual.[21] The twist in H_2L^I from the sterically hindered t-butyl groups causes a lack of symmetry in the binding pocket. The V-O1 and V-O2 bond distances of 1.929(2) and 1.930(2) Å respectively are comparable to literature (1.91-1.95 Å) which have greater variety than the vanadium nitrogen distances.[21]

Table 1. Crystallographic data and details of data collection for $[H_2L^I]$, $UO_2[L^I](H_2O)$, $Cu[L^I]$, $VO[L^I]$, $Zn[L^I](CH_3OH)$, and $Fe[L^I]$-O-$Fe[L^I]$.

	$[H_2L^I]$•½EtOAc	$UO_2[L^I](H_2O)$•$2H_2O$*	$Cu[L^I]$*	$VO[L^I]$	$Zn[L^I](CH_3OH)$	$Fe[L^I]$-O-$Fe[L^I]$
Formula	$C_{44}H_{54}N_4O_3$	$C_{42}H_{54}N_4O_7U$	$C_{42}H_{48}N_4O_2Cu$	$C_{42}H_{48}N_4O_3V$	$C_{43}H_{53}N_4O_3Zn$	$C_{92}H_{112}Fe_2N_8O_7$
MM (g/mol)	682.91	955.85	704.39	707.82	738.31	1553.6
Crys. size (mm)	0.8x0.15x0.02	0.1x0.4x0.2	0.4x0.09x0.05	0.6x0.08x0.08	0.2 x 0.1 x 0.1	0.1x0.1x0.08
Crystal system	monoclinic	monoclinic	triclinic	triclinic	triclinic	monoclinic
space group	$P2_1/n$	$P2_1/n$	P1	$P\bar{1}$	$P\bar{1}$	C2/c
volume ($Å^3$)	3901.1(2)	5047.6(9)	1836.17(7)	2120.59(14)	2193.30(19)	8520.7(2)
a (Å)	6.2424(2)	18.0541(18)	9.9751(2)	10.5213(4)	9.3102(5)	18.9491(3)
b (Å)	22.8992(7)	13.4873(13)	12.6630(3)	12.7581(5)	15.1537(7)	41.3420(7)
c (Å)	27.3844(8)	20.820(2)	14.8623(3)	16.9448(6)	16.4769(8)	13.8422(2)
α (deg)	90	90	93.610(1)	77.715(1)	105.875(2)	90
β (deg)	94.704(1)	97.380(3)	96.835(1)	74.447(1)	100.257(2)	128.2090(10)
γ (deg)	90	90	98.716(1)	79.226(1)	91.511(2)	90
Z	4	4	2	2	2	4
ρ (calc. g cm^{-3})	1.1626	1.263	1.2658	1.1084	1.1179	1.136
μ (mm^{-1})	0.073	3.271	0.636	0.272	0.606	0.399
F(000)	1464.6	1892	737.9	750.9	864.9	3088
temp (K)	180(4)	296(2)	296(2)	296(2)	180(2)	180(2)
total no. reflec.	75008	39876	54883	35450	43775	50375
unique reflec.	6196	8274	15270	7239	8341	9764
Largest diff. peak and hole (e.A^{-3})	0.35/-0.28	2.74/-1.86	0.76/-0.28	0.32/-0.32	0.59/-0.61	0.74/-0.55
Final R indices [$I > 2\sigma(I)$]	R1 = 0.0453, wR2 = 0.1081	R1 = 0.0621, wR2 = 0.1816	R1 = 0.0375, wR2 = 0.0952	R1 = 0.0492, wR2 = 0.1321	R1 = 0.0467, wR2 = 0.1086	R1 = 0.0557, wR2 = 0.1510
GOF	1.067	1.134	1.016	1.059	1.064	1.033
CCDC	1452415	1019622	1019624	1452867	1452244	1018600

*See reference 16

This complex forms pseudo two dimensional sheets involving a dimer held together by π–π interactions in the solid state. These sheets are separated by 12.55 Å. The π–π distance between the P1-P2 rings on phenazine of the dimer is 3.36 Å. These electron rich systems prefer off-center parallel π–π stacking. The M–P3 distance between the dimer phenazine rings is 3.235 Å, suggesting possible metal backbonding to the pi system of the ligand.

Table 2. Selected bond distances (Å) and bond angles (deg) for $[H_2L^I]$, $UO_2[L^I](H_2O)$, $Cu[L^I]$, $VO[L^I]$, $Zn[L^I](CH_3OH)$, and $Fe[L^I]$-O-$Fe[L^I]$.

	$[H_2L^I]$	$Cu[L^I]$	$UO_2[L^I]$	$VO[L^I]$	$Zn[L^I]$	$Fe[L^I]$-O-$Fe[L^I]$
M-N1	--	1.92	2.54	2.05	2.07	2.11
M-N2	--	1.94	2.56	2.05	2.08	2.10
M-O1	--	1.92	2.27	1.93	1.95	1.92
M-O2	--	1.89	2.24	1.93	1.97	1.91
M-O3	---		2.45	1.59	2.11	1.76
O1-N1	2.59	2.79	2.73	2.74	2.85	2.76
N1-N2	2.70	2.58	2.71	2.59	2.65	2.62
N2-O2	2.61	2.81	2.75	2.75	2.85	2.77
O1-O2	3.41	2.66	4.42	2.65	2.89	2.80
O1-N2	3.64	3.85	4.43	3.76	3.99	3.87
O2-N1	4.23	3.81	4.40	3.83	3.92	3.85
O1-M1-N1	--	93.3	68.9	86.9	89.9	86.1
N1-M1-N2	--	83.8	64.1	78.3	79.5	76.8
N2-M1-O2	--	94.5	69.5	87.3	89.6	87.1
O2-M1-O1	--	88.7	157.5	86.9	94.9	93.9
M1-O3-M1	--	--	--	--	--	161.5
M1-Lplane*	--	0.178	1.96	0.983	0.837	0.583

L-plane defined by C4-C21-C22-C31

Complex $Zn[L^I](CH_3OH)$ crystallizes in the triclinic space group $P\bar{1}$ and is shown in **Figure 2**. This complex has a square pyramidal geometry around the zinc atom with a coordinating neutral methanol molecule. This is observed by the close to 90° bond angles of the zinc to the O-N-N-O ligand donor atoms, O1-Zn-N1, N1-Zn-N2, N2-Zn-O2, O2-Zn-O1 are 89.90(11), 79.46(11), 89.55(10), 94.88(10)° respectively. These bond angles are comparable to previously reported zinc structures with coordinating methanol or pyridine solvent (79.0-95.5°).[22a,b] The oxygen (O3) from the methanol is also approximately 90° from the equatorially bound ligand with O3-Zn-O1, O3-Zn-O2, O3-Zn-N1, O3-Zn-N2 angles of 101.02(11), 98.79(11), 95.01(10) and 105.18(11)° respectively. This coordination solvent is quite labile, and the zinc metal quickly dissociates from the ligand under acidic conditions. The zinc atom binds less securely than the copper in the tetradentate binding pocket with Zn-N1, Zn-N2, Zn-O1, Zn-O2 bond distances of 2.074(3), 2.076(3), 1.954(2), and 1.965(2) Å, respectively. These bond lengths are within ± 0.03 Å of the previously reported Zn(salphenzine)(DMSO) complex,[23] and within standard lengths of previously reported zinc salophen structures(Zn-O 1.93-1.97 Å and Zn-N 2.04-2.09 Å).[22a-c]

Complex $Fe[L^I]$-O-$Fe[L^I]$ crystallizes in the monoclinic space

View Article Online
DOI: 10.1039/C6DT02389D

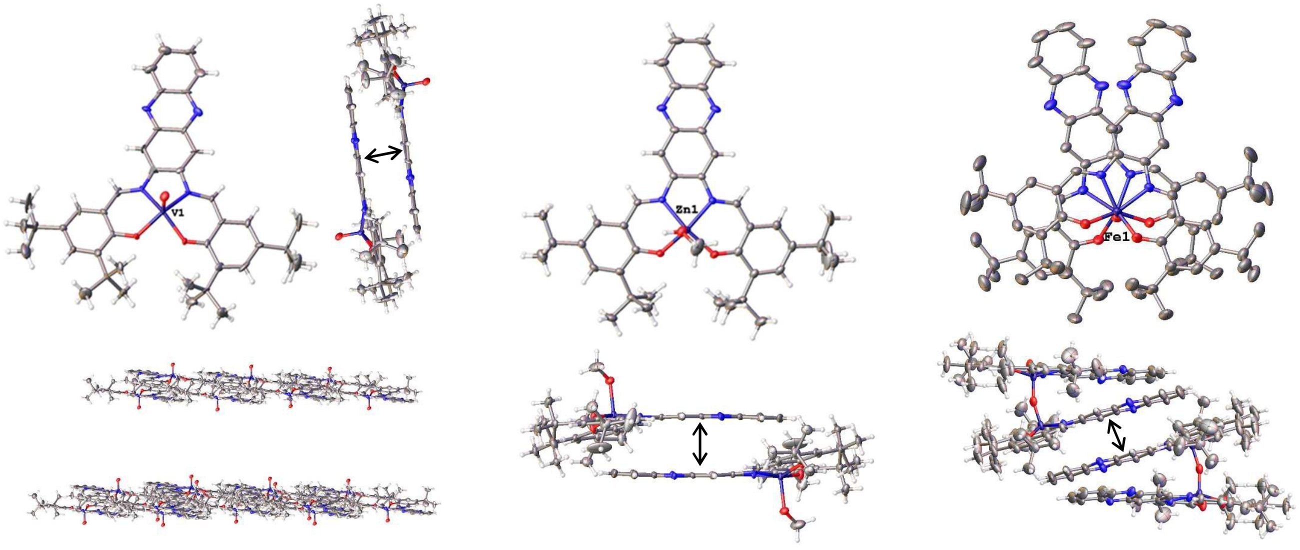

VO[L^{I}] Zn[L^{I}](CH_3OH) Fe[L^{I}]-O-Fe[L^{I}]

Figure 2.Projections of VO[L^{I}], Zn[L^{I}](CH_3OH), and Fe[L^{I}]-O-Fe[L^{I}] complexes. Solid-state dimers and pseudo 2-D sheets are also shown. Transition metal shown in purple, carbon atoms shown in grey, nitrogen shown in blue, oxygen shown in red, hydrogen (when not omitted for clarity) are shown in white. All interstitial solvents were removed for clarity.

group C2/c and is shown in **Figure 2**. The iron (III) atom is in a square pyramidal geometry with the axial position being occupied by a bridging oxo group to a second, symmetry related, iron-ligand complex. This phenomenon is well documented in the literature, with 814 examples of mixed nitrogen and oxygen donor ligands with μ-oxo geometries, and 28 examples of salen ligands with μ –oxo geometries reported in the Cambridge Crystallographic Data Center (CCDC).[24] The iron atom binds in the tetradentate binding pocket, but has the most distortion from square pyramidal as compared to the vanadyl and zinc structures with O1-Fe-N1, N1-Fe-N2, N2-Fe-O2, O2-Fe-O1 bond angles of 76.81(9), 87.14(10), 86.12(7), and 93.85(9)° respectively. These angles are within other examples in the literature (76.3-94.5°).[25a,b] The Fe-N1, Fe-N2, Fe-O1, and Fe-O2 bond distances are also the longest of the transition metal structure in this M[L^{I}] series with lengths of 2.1105(18), 2.100(3), 1.9216(17), and 1.906(2) Å, respectively. These distances are comparable to other Fe-salen dimers and elongated in comparison to some less sterically hindered complexes.[25a-e] Of note is the lack of π-stacking in the dimer, and the Fe1-O3-Fe1 angle of 161.50(16)° which is comparable to other μ-oxo species[25a,b] but is well below the stereotypical limits observed of 1.75-1.80°.[25a] This can be explained by steric hindrance of the substituted aldehyde moieties. The π–π distance between the P1-P2 rings on the external dimer phenazine rings is 3.35 Å. The metal is 3.172 Å above the P3 ring.

Structurally, the uranyl metal complex UO_2[L^{I}] is most similar to the ligand geometry. The axial positions of the uranium coordination sphere are occupied by the two oxo "-yl" groups of the uranyl subunit. The uranium atom is bound further out in the pocket than the transition metals. These bond distances are consistently 0.5 Å longer than the transition metal analogues (**Table 2**). This puckering of the ligand causes a shift from a planar backbone and results in the uranium atom being 1.954(9) Å above the plane of the ligand as defined by C4-C21-C22-C31. This puckering, highlighted in **Figure 3**, is the explanation of the spectroscopic distinction

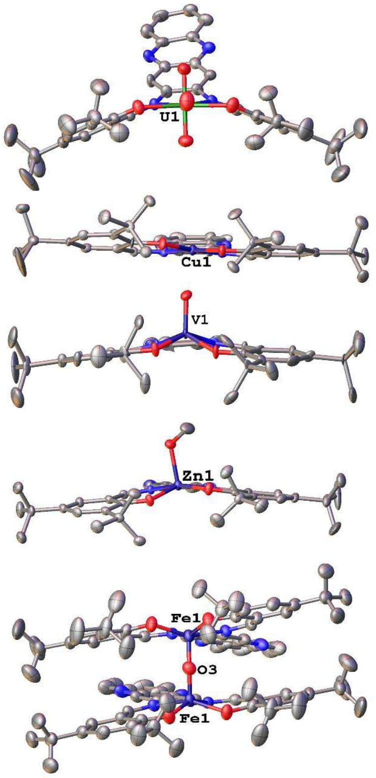

Figure 3. Projections of M[L^{I}] series highlighting the pucker of the tetradentate binding pocket. Carbon atoms shown in grey, nitrogen shown in blue, oxygen shown in red, transition metals shown in purple, uranium shown in green, and hydrogen omitted for clarity.

View Article Online
DOI: 10.1039/C6DT02389D

between uranyl and the transition metal analogues. The planarity of the ligand, regardless of the steric bulk in the 3-position of the aldehyde, for the transition metal complexes was surprising. The planarity of the transition metal structures can be observed most distinctly by the distance of the Cu-L_{plane} distance of 0.178(3) Å. The VO[L^{I}] structure is second only to the uranyl structure in distance from metal to ligand plane with V-L_{plane} distance of 0.967(7) Å. The Zn-L_{plane} distance of 0.837(2) Å above the ligand plane is accompanied by a twist in the O-N-N-O pocket, explaining the lability observed in this metal complex as compared to the other analogues. The iron atom is closer to the plane of the ligand, however, than Zn[L^{I}](CH_3OH) or VO[L^{I}] structures, with a Fe-L_{plane} distance of 0.583(2) Å. The iron atom is closer to the ligand plane than the other structures, while simultaneously having longer bond lengths suggesting that the *tert*-butyl groups in the 3 and 3' positions keep the pocket open wider than is strictly necessary for this metal centre.

Spectroscopy

All UV measurements were done using a Cary 50 spectrometer and with pyridine as a solvent due limitations of solubility. The λ_{max} values and molar absorptivities of the charge transfer bands for M[L^{I}] complexes are listed in **Table 3**. Ligand [H_2L^{I}] exhibits and absorption band at 424 nm. Upon 1:1 binding of UO_2^{2+} a 60 nm hypsochromic shift of the π-π* excitation to 364 nm is observed. A charge transfer band with a maximum absorbance at 470 nm (ε = 1.95 x 10^4 cm^{-1} M^{-1}), a separation of 48 nm from the original ligand peak, and a shoulder at 520 nm are also observed in UO_2[L^{I}]. By comparison, the Cu[L^{I}] complex, exhibits a hypsochromic shift of the ligand peak of 24 nm and a charge transfer band at 521 nm (ε = 1.95 x 10^4 cm^{-1} M^{-1}) with a shoulder at 470 nm, a peak separation of 98 nm.

Compound [H_2L^{I}] was complexed with other earth abundant transition metals Cu^{2+}, Zn^{2+}, Fe^{3+}, Co^{2+}, Ni^{2+}, and VO^{2+} as shown in **Figure 4**. The complex Zn[L^{I}] exhibits a charge transfer band at 520 nm (ε = 1.51 x 10^4 cm^{-1} M^{-1}) with a hypsochromic shift of the ligand peak by 37 nm. The Fe[L^{I}]-O-Fe[L^{I}] complex has a charge transfer band at nm (9.26 x 10^3 cm^{-1} M^{-1}) after the templation condensation reaction, but shows no reaction when the free metal salt is introduced. The presence of a Co^{2+} ion (Co[L^{I}]) induced a charge transfer band at 517 nm (ε = 1.35 x 10^4 cm^{-1} M^{-1}), a peak separation of 93 nm, and a hypsochromic shift of the ligand peak by 12 nm. Introduction of the Ni^{2+} ion (Ni[L^{I}]) induced a charge transfer band at 509 nm (ε = 1.42 x 10^4 cm^{-1} M^{-1}), a peak separation of 85 nm, with a shoulder at 570 nm which was not present in any of the other complexes. A hypsochromic shift of 10 nm, along with an additional high energy peak was also observed. Complex VO[L^{I}], which is the least likely contaminant in waste water samples, has a maximum at 471 nm (ε = 1.47 x 10^4 cm^{-1} M^{-1}). The binding of vanadyl is much slower, over 24 hours, than the other transition metals. The UV-Vis spectra of compounds [H_2L^{I}] and M[L^{I}] complexes are shown in **Figure 4**. The UO_2[L^{I}] complex has greater than 30 nm of separation from all the transition metals, save VO[L^{I}], and 50 nm separation between the ligand and complex absorbance.

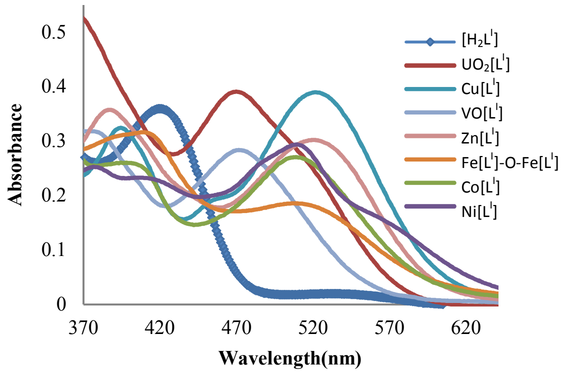

Figure 4. UV-Vis spectral changes of M[L^{I}] complexes at 20 μM concentration in pyridine.

Table 3. UV-Visible data for M[L^{I}]complexes and free base [H_2L^{I}], 20 μM in pyridine solution.

	λ (nm)	ε (x 10^4 cm^{-1} M^{-1})
[H_2L^{I}]	420	1.80
UO_2[L^{I}]	369	2.64
	470	1.95
Cu[L^{I}]	394	1.62
	455	0.959
	521	1.95
VO[L^{I}]	375	1.59
	471	1.41
Zn[L^{I}]	387	1.79
	521	1.51
Fe[L^{I}]-O-Fe[L^{I}]	408	1.58
	511	0.926
Co[L^{I}]	338	1.88
	403	1.29
	509	1.35
Ni[L^{I}]	374	1.22
	408	1.08
	509	1.42

Electrochemistry

Cyclic voltammagrams for the salphenazine compounds [H_2L^{I}], UO_2[L^{I}], and Cu[L^{I}] are shown in Figure 5a. The cyclic voltammagrams of salqu compounds (**Scheme 2**) [H_2L^{II}], UO_2[L^{II}], and Cu[L^{II}] are compared in **Figure 5b**. The change in stability of ligand oxidation was also investigated. All compounds were studied at 1.0 mM concentration in a dichloromethane solution with 0.100 M of tetra-n-butylammounium perchlorate electrolyte. Experiments were run with a scan rate of 0.10-1.50 V s^{-1} on a platinum working electrode vs. a Ag/AgCl reference electrode and a platinum wire counter electrode.

View Article Online
DOI: 10.1039/C6DT02389D

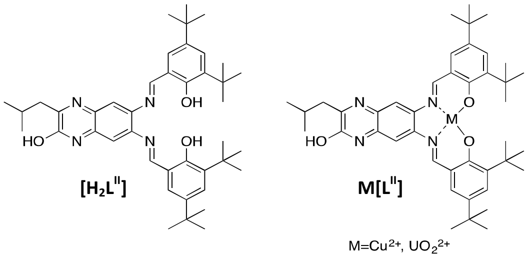

Scheme 2. Salqu $[H_2L^{II}]$ and salqu complexes $M[L^{II}]$, synthesized according to literature procedure.

The salphenazine $[H_2L^I]$ ligand shows four oxidation peaks, at $E_p^{ox,a}$ = 1.21 V, $E_p^{ox,b}$ = 1.33 V, $E_p^{ox,c}$ = 1.56 V, and $E_p^{ox,d}$ = 1.77 V, none of which are reversible. This result suggests $[H_2L^I]$ can stabilize not only the cationic radical on the phenol groups, but can further oxidize. Reduction peaks were not present in $[H_2L^I]$. The same is not true for salqu $[H_2L^{II}]$; two oxidation peaks at $E_p^{ox,a}$ =1.17 V and $E_p^{ox,b}$ = 1.61 V and two reduction peaks at $E_p^{red,a}$ = -0.085 V and $E_p^{red,b}$ = -0.62 V which are all not reversible are observed. The two oxidation peaks are indicative of a phenoxyl radical formed from a single electron oxidation. The two reduction peaks are indicative of reduction of the imine nitrogen.

Two of the oxidation peaks from $[H_2L^I]$ are absent from the complex $[H_2L^{II}]$ voltammagram. Two oxidation peaks at $E_p^{ox,a}$ = 1.19 V and $E_p^{ox,b}$ = 1.52 V remain and are now quasireversible with separation of the anodic of cathodic peaks of 30 and 150 mV respectively shown in **Figure 5b**. One oxidation peak of $[H_2L^I]$ is not observed in the salphenazine complex $Cu[L^I]$ which has oxidation peaks at $E_p^{ox,a}$ = 1.17 V, $E_p^{ox,b}$ = 1.30 V, $E_p^{ox,c}$ = 1.72 V. The three remaining oxidation peaks do not shift in oxidation potential from the ligand by more than $E_{1/2}$ = 0.050 V suggesting minimal stabilization of the phenoxyl radicals formed upon oxidation by the copper ion. The oxidation peaks in $UO_2[L^I]$ become quasi reversible suggests that the phenoxyl radicals are stabilized by the uranyl ion. A new reduction peak at E_p^{red} = 0.15 V is observed in the complex $UO_2[L^I]$ that is not present in the free base, suggesting that the uranyl ion stabilizes the π–system enough to reduce the imine nitrogen that did could occur in the free base $[H_2L^I]$ (See supplemental information).

The oxidation peaks in the salqu complexes $UO_2[L^{II}]$ and $Cu[L^{II}]$ become quasi-reversible suggesting that the phenoxyl radicals are stabilized by the metal ions. Complex $Cu[L^{II}]$ has two single electron oxidation peaks at $E_p^{ox,a}$ = 1.06 V $E_p^{ox,b}$ = 1.27 V with anodic and cathodic peak potential separation values in the range of 50 – 70 mV. Complex $UO_2[L^{II}]$ has two single electron oxidation peaks at $E_p^{ox,a}$ = 1.04 V $E_p^{ox,b}$ = 1.33 V with anodic and cathodic peak potential separation values in the range of 20 – 50 mV that seem to be quasi-reversible at best. Both metal complexes show reversible ligand oxidation peaks at $E_p^{ox,a}$ and $E_p^{ox,b}$, indicative of phenol type radical oxidation of the ligand.26 The average shifts in the oxidation potential from the free base $[H_2L^{II}]$ of $E_{1/2}$ = 0.12 and $E_{1/2}$ = 0. 032 observed in complexes $UO_2[L^{II}]$ and $Cu[L^{II}]$ suggest moderate stabilization of the phenoxyl radical. A third cathodic peak $E_p^{red,c}$ = 0.82 V present in complex $Cu[L^{II}]$ which may be attributed to a Cu(III)-phenolate species that is present simultaneously with the Cu(II)-phenoxyl radical species.

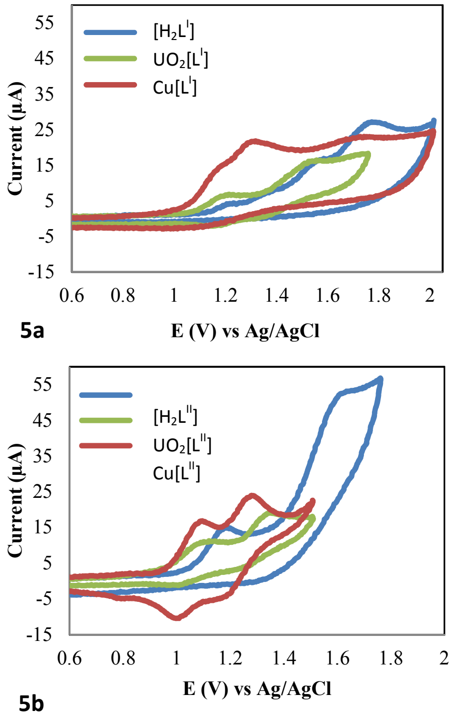

Figure 5a. Cyclic Voltammagram of $[H_2L^I]$, $UO_2[L^I]$, and $Cu[L^I]$. Conditions: 0.5 mM ligand in dichloromethane, room temperature, tetra-n-butylammonium perchlorate (0.1 M) as electrolyte with a 0.10 V s^{-1} scan rate. **Figure 5b**. Cyclic Voltammagram of $[H_2L^{II}]$, $UO_2[L^{II}]$, and $Cu[L^{II}]$. Conditions: 1.0 mM ligand in dichloromethane, room temperature, tetra-n-butylammonium perchlorate (0.1 M) as electrolyte with a 0.10 V s^{-1} scan rate.

Complex $UO_2[L^I]$ resulted in two reduction peaks, at $E_p^{red,a}$ = -1.57 V and $E_p^{red,b}$ = -2.18 V, both of which are visibly quasireversible in **Figure 6**. The $UO_2[L^{II}]$ complex, has a reduction peak at $E_p^{red,a}$ = -1.87 V and $E_p^{red,b}$ = -2.11 V. The reduction of U(VI) to U(V) in UO_2[salophen] occurs at -1.67 V in pyridine and -1.55 in DMSO.[27] Complex $UO_2[L^{II}]$ has an ΔE= 0.20 V and ΔE = 0.32 V for the U(VI)/U(V) redox couple, revealing a better stabilization of the uranyl complex in the salqu ligand, even without the presence of a coordinating solvent, than in previous salophen complexes. This stabilization is not present in the $UO_2[L^I]$ complex with a $\Delta E_{1/2}$ = 0.02 V. The second reduction peaks may be due to not only a reduction of uranium to the pentavalent uranyl cation, but subsequent disproportionation to U(IV) and U(VI) or a rearrangement of the uranium geometry. If a coordinating solvent is removed from the coordination sphere, an additional oxidation peak may present itself.

Conclusions

View Article Online
DOI: 10.1039/C6DT02389D

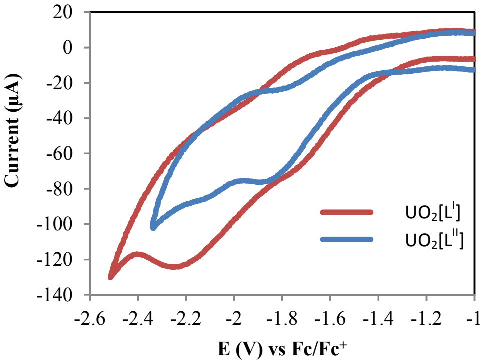

Figure 6. Cyclic Voltammagram of $UO_2[L^I]$ and $UO_2[L^{II}]$. Conditions: 0.5 mM complex in dichloromethane, room temperature, tetra-n-butylammonium perchlorate (0.1 M) as electrolyte with the ferrocene redox couple as an internal standard.

The salphenazine ligand, with the O-N-N-O salen type bonding motif, has been synthesized and characterized in the presence of various first row transition metals and uranium in the most common oxidation state in aqueous solution (UO_2^{2+}). Complexes have been characterized by x-ray crystallography and UV-visible spectroscopy, revealing the extended π-conjugation of these ligands results in differentiation of a uranyl signal as compared to these transition metal contaminants. The solid-state characterization of this series provides insight to the preferred coordination environment of uranyl in these conjugated systems. The π–π stacking of all the observed systems is within the confines of typical graphene stacking distance of 3.21-3.50 Å. The metal centres often are within 3.0-3.2 Å above a conjugated ring, suggesting possible metal backbonding to the ring system. These insights can guide further design for ligands with extended conjugation to be used as on-site actinide chemosensors. The free bases, compounds $[H_2L^I]$ and $[H_2L^{II}]$, along with the uranyl and copper complexes, $UO_2[L^I]$, $Cu[L^I]$, $UO_2[L^{II}]$, and $Cu[L^{II}]$, have been characterized by cyclic voltammetry. The extended π-conjugation that is deemed responsible for differentiation between metals in the spectroscopy does not necessarily translate into increased stability of the U(V)/U(VI) redox couple, which may provide a secondary sensing method for chemosensors of this type.

Acknowledgements

This work was supported in part by the Defence Threat Reduction Agency, Basic Research Award # HDTRA1-11-1-0044 to Auburn University. We gratefully acknowledge John Gorden for helpful discussion and x-ray diffraction.

References

1 Corner, A., Venables, D., Spence, A., Poortinga, W., Demski, C., Pidgeon, N. *Energ. Policy* **2011**, *39*, 4823; Karp, J. S., Surti, S., Daube-Witherspoon, M. E., Meuhllehner, G. *J. Nucl. Med.* **2008**, *49*, 462; Youinou, G. J. *Renew. Sust. Energ. Rev.* **2016**, *53*, 1626.

2 Snow, M. S., Snyder, D. C., Clark, S. B., Kelley, M., Delmore, J. E. *Environ. Sci. Technol.* **2015**, *49*, 2741.

3 Gorden, A. E. V., Xu, J., Raymond, K. N., Durbin, P. *Chem. Rev.* **2003**, *103*, 4207.

4 Sessler, J., Melfi, P., Pantos, G. *Coord.. Chem. Rev.* **2006**, *250*, 816; Gorden, A. E., DeVore, M. A., II, Maynard, B. A. *Inorg. Chem.* **2013**, *52*, 3445.

5 Li, Y., Lee, T., Weerasiri, K., Wang, T., Buss, E. E., McKee, M. L., Gorden, A. E. V. *Dalton Trans.* **2014**, *43*, 13578; Weerasiri, K. C., Gorden, A. E. V. *Eur. J. Org. Chem.* **2013**, 1546; Chen, T., Cai, C. *Synth. Commun.* **2015**, *45*, 1334; North, M., Quek, S. C. Z., Pridmore, N. E., Whitwood, A. C., Wu, X. *ACS Catalysis* **2015**, *5*, 3398.

6 Nishat, N., Rasool, R., Parveen, S., Khan, S. A. *J. Appl. Polym. Sci.* **2011**, *122*, 2756; Murtinho, D., da Rocha, Z. N., Pires, A. S., Jiménez, R. P., Abrantes, A. M., Laranjo, M., Mamede, A. C., Casalta-Lopes, J. E., Botelho, M. F., Pais, A. C., Nunes, S. C. C., Burrows, H. D., Costa, T., Silva Serra, M. E. *Appl. Organomet. Chem.* **2015**, *29*, 425.

7 Peng, Q., Xie, M., Huang, Y., Lu, Z., Cao, Y. *Macromol. Chem. Phys.* **2005**, *206*, 2373; Hwang, K. Y., Lee, M. H., Jang, H., Sung, Y., Lee, J. S., Kim, S. H., Do, Y. *Dalton Trans.* **2008**, 1818; Ren, M., Xu, Z.-L., Bao, S.-S., Wang, T.-T., Zheng, Z.-H., Ferreira, R. A. S., Zheng, L.-M.; Carlos, L. D. *Dalton Trans.* **2016**.

8 a) Zhou, D., Sun, C., Chen, C., Cui, X., Li, W. *J. Mol. Struct.* **2015**, *1079*, 315. b) Cheng, J., Wei, K., Ma, X., Zhou, X., Xiang, H. *J. Phys. Chem. C* **2013**, *117*, 16552; c) Lin, H.-Y., Chen, T.-Y., Liu, C.-K., Wu, A.-T. *Luminescence* **2016**, *31*, 236.

9 Winn, J. P., Aleksandra, Goldup, S. M. *J. Am. Chem. Soc.* **2013**, *135*, 13318; Ronson, T. K., Zarra, S., Black, S. P., Nitschke, J. R. *Chem. Commun.* **2013**, *49*, 2476; Beves, J. E. B., Barry, A., Campbell, C. J., Leigh, D. A.; McBurney, R. T. *Angew. Chem. Int. Ed.* **2011**, *50*, 9260; Cheng, H. M., Leigh, D. A., Maffei, F., McGonigal, P. R., Slawin, A. M. Z., Wu, J. *J. Am. Chem. Soc.* **2011**, *133*, 12298.

10 Whicker, F. W., Schultz, V. *Radioecology: Nuclear Energy and the Environment*; CRC Press, Inc.: Boca Raton, Florida, 1982; Vol. 1.

11 Vega, F. A., Covelo, E. F., Andrade, M. L. *J. Colliod Interf. Sci.* **2005**, *298*, 582.

12 Sessler, J. L., M, P. J., Seidel, D., Gorden, A. E. V., Ford, D. K., Palmer, P. D., Tait, C. D. *Tetrahedron* **2004**, *60*, 11089.

13 a) Wu, X., Bharara, M. S., Bray, T. H., Tate, B. K., Gorden, A. E. V. *Inorg. Chim. Acta* **2009**, *362*, 1847; b) Bharara, M. S., Heflin, K., Tonks, S., Strawbridge, K. L., Gorden, A. E. V. *Dalton Trans.* **2008**, *22*, 2966. c) DeVore II, M. A., Kerns, S. A., Gorden, A. E. V. *Eur. J. Inorg. Chem.* **2015**, *2015*, 5708.

14 Mikhalyova, E. A., Yakovenko, A. V., Zeller, M., Gavrilenko, K. S., Lofland, S. E., Addison, A. W., Pavlishchuk, V. V. *Inorg. Chim. Acta* **2014**, *414*, 97.

15 Bharara, M. S., Strawbridge, K., Vilsek, J. Z., Bray, T. H, Gorden, A. E. V. Inorg. Chem. **2007**, *46*, 8309; Salassa, G., Ryan, J. W., Escudero-Adan, E. C., Kleij, A. W. *Dalton Trans.* **2014**, *43*, 210.

16 Maynard, B. A., Brooks, J. C., Hardy, E. E., Easley, C. J., Gorden, A. E. V. *Dalton Trans.* **2015**, *44*, 4428.

17 Wu, X., Gorden, A. E. V. *J. Comb. Chem.* **2007**, *9*, 601.

18 Sheldrick, G. M. *Acta Crystallogr., Sect. A: Found. Crystallogr.* **2008**, *A64*, 112.

19 Bruker, Bruker AXS Inc.: Madison, Wisconsin, USA, 2001.

20 Dolomanov, O. V., Bourhis, L. J., Gildea, R. J., Howard, J. A. K., Puschmann, H. *J. Appl. Cryst.* **2009**, *42*, 339.

21 Zamian, J. R., Dockal, E. R., Castellano, G., Oliva, G. *Polyhedron* **1995**, *14*, 2411; Weberski Jr, M. P., McLauchlan, C. C., Hamaker, C. G. *Polyhedron* **2006**, *25*, 119; Zabierowski, P., Szklarzewicz, J., Grybos, R., Modryl, B., Nitek, N. *Dalton Trans.* **2014**, *43*, 17044.

View Article Online
DOI: 10.1039/C6DT02389D

22 a) Morris, G. A., Zhou, H., Stern, C. L., Nguyen, S. T. *Inorg. Chem.* **2001**, *40*, 3222; b) Liuzzo, V., Oberhauser, W., Pucci, A. *Inorg. Chem. Commun.* **2010**, *13*, 686. c) Germain, M. E., Vargo, T. R., Khalifah, P. G., Knapp, M. J. *Inorg. Chem.* **2007**, *46*, 4422.

23 Salassa, G., Ryan, J. W., Escudero-Adan, E. C., Kleij, A. W. Dalton Trans. **2014**, *43*, 210.

24 Allen, F. H. *Acta Cryst.* **2002**, *B58*, 380.

25 a) Mayilmurugan, R., Stoeckli-Evans, H., Sleresh, E., Palaniandavar, M. *Daton Trans.* **2009**, *26*, 5101; b) Rusere, L. N., Shalumova, T., Tanski, J. M., Tyler, L. A. *Polyhedron* **2009**, *28*, 3804; c) Jana, S., Chatterjee, S., Chattopadhyay, S. *Polyhedron* **2012**, *48*, 189; d) Veauthier, J. M., Cho, W.-S., Lynch, V. M., Sessler, J. L. *Inorg. Chem.* **2004**, *43*, 1220; e) Whiteoak, C. J., Rosales, R. T. M., White, A. J. P., Britovsek, G. J. P. *Inorg. Chem.* **2010**, *49*, 11106.

26 Asami, K., Takashina, A., Kobayashi, M., Iwatsuki, S., Yajima, T., Kochem, A., Gastel, M. V., Tani, F., Kohzuma, T., Thomas, F., Shimazaki, Y. *Dalton Trans.* **2014**, *43*, 2283.

27 Mizuoka, K., Kim, S. Y., Hasegawa, M., Hoshi, T., Uchiyama, G., Ikeda, Y. *Inorg. Chem.* **2003**, *42*, 1031; Nocton, G., Horeglad, P., Vetere, V., Pecaut, J., Dubois, L., Maldivi, P., Edelstein, N., Mazzanti, M. *J. Am. Chem. Soc.* **2010**, *132*, 495.